Robotic Deployment of Embedded Strain Sensors in Precast Tunnel Segments

Tresor Tshimbombo*[a], Marcus Perry [a], Hamish Dow [a], Jack McAlorum [a], Chris Hoy [b]
Chrysoula Litina[c]

***Abstract*— The paper demonstrates the robotic deployment of sensor nodes into precast concrete tunnel segments during manufacturing. Magnetic embeddable sensor nodes based on vibrating wire strain gauges were deployed on a steel precast segment mould using a six-axis collaborative robot at the lab scale. Robotic sensor deployment proved to be significantly more accurate and consistent than manual sensor deployment methods. On average, positional and angular errors in sensor placement were reduced by 85% when using robotic deployment. The strain transfer coefficients for robotically embedded sensors were evaluated using mechanical bending tests and a finite element model. Strain transfers across a population of 10 segments were found to be 0.93 ± 0.012 in the longitudinal direction, and 0.567 ± 0.011 in the transversal direction. The repeatability of strain measurements within these segments was also confirmed, with low coefficient of variation values of 1% for longitudinal strains and 1.9% for transversal strains. The work presented in this paper underscores the measurement performance enhancements that can result from using robotics for sensor deployment in precast manufacturing environments. This could translate to a lower uncertainty and risk for civil asset managers and structural health monitoring practitioners.**

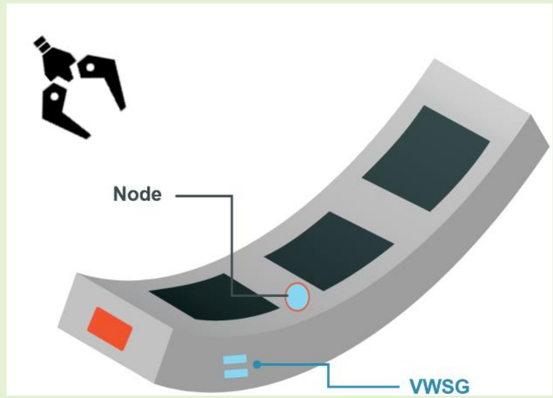

1

***Index Terms*— concrete structures, robotics, automation, sensor deployment, vibrating wire strain gauges**

I. INTRODUCTION

SENSING and automation are increasingly being adopted for the manufacturing and monitoring of critical civil infrastructure, such as tunnels [1]. Tunnels are costly and require a meticulous approach to asset management across every phase of their lifecycle [2]. From the initial planning to the construction phase through to their operational years, tunnels must be continually monitored to ensure safety, durability, cost-efficiency and resilience.

The field of Structural Health Monitoring (SHM) is now well-established in civil engineering, as evidenced by numerous studies outlining its successful deployment in tunnels [3]-[17]. In most of the mentioned studies, sensors are installed on-site after construction during the fit-out phase. However, there are cases where sensors are installed before construction to monitor the structure's behaviour during and after the build [18]-[20]. In these applications, the system is typically set up to capture the global behaviour of the entire structure or sections of the structure. The structural behaviour of individual elements such as precast segments linings, before they are incorporated into the structure, are not considered.

However, pre-construction flexural loads are generally more critical for steel fibre reinforced concrete (SFRC) tunnel segments design than construction and service loads. Unlike traditional reinforced concrete, SFRC presents very low resistance to tensile strains, more prevalent during the preconstruction phase, particularly during the handling and transportation of the segments before installation.

To address the limitations of current sensor deployment practices, we propose automating sensor installation during the manufacturing of precast tunnel elements, rather than waiting until after construction. This approach not only makes it possible to capture the preconstruction segment behaviour but also leverages the repetitive nature of manufacturing precast tunnel segments, making them ideal candidates for robotic sensor integration. Precast manufacturing plants offer a controlled environment for sensor deployment, enabling a more comprehensive collection of real-time structural data of segments throughout their lifecycles.

In this paper, we address the challenges of manual sensor deployment in segmental tunnels by introducing a robotic approach for instrumenting tunnel segments during the precast

a University of Strathclyde, Department of Civil and Environmental Engineering, 75 Montrose Street, G1 1JQ, Glasgow, United Kingdom
b COWI UK Ltd, 5Th Floor 310 St Vincent Street, Glasgow G2 5RG, Glasgow, United Kingdom
c National Highways, Woodlands Manton Lane, Manton Industrial Estate, Bedford, MK41 7LW, United Kingdom

This article has been accepted for publication in IEEE Sensors Journal. This is the author's version which has not been fully edited and content may change prior to final publication. Citation information: DOI 10.1109/JSEN.2025.3559405

manufacturing stage. Sensor nodes with Vibrating Wire Strain Gauges (VWSGs) are deployed using a six-axis robot onto an empty formwork. Once the concrete is poured, the sensors become embedded in the segments, resulting in lab-scale instrumented tunnel segments. We discuss the methodology, key design aspects of the sensors, their packaging, and the automation process, along with an analysis of placement errors and strain transfer.

To the best of our knowledge, this paper presents the first demonstration of robotic deployment and characterization of embedded sensor nodes in a precast tunnel segment at the lab scale. This research has the potential not only to enhance safety, efficiency, and cost-effectiveness in tunnel construction, operation and maintenance but also paves a way for a broader adoption of automation in the construction industry.

A. BACKGROUND

1) *Automation in the precast concrete industry*

Despite its increasing adoption in other manufacturing industries, such as aeronautics, automobiles, and food, the use of robots in construction and civil engineering is still in its early stages [21]-[22]. Possible reasons for this may include a lack of adapted robotic solutions or resistance to innovation. The construction industry has seen limited development of robotic applications since the 1970s, with descriptions of various applications available in [23]-[26].

Precast manufacturing is one exception. The production of concrete precast elements occurs in a more controlled environment compared to on-site operations. The extensive use of machinery for crucial operations like lifting, transporting, and concrete mixing not only enhances safety but also optimizes production efficiencies. This manufacturing environment is well-suited for integrating robotics into the process.

Two general production methods are typically employed for fabricating precast elements. The first method, known as the static mode, employs stationary moulds throughout the process [24]. The second method uses mobile moulds mounted on carousel palettes [24]. In both processes, the prefabrication steps are similar. The first step involves preparing the mould (cleaning, applying demoulding production, installing reinforcement, and other accessories). The next step is the casting and curing of concrete, and the final step is transportation to a storage facility before delivery [24]. Robotics have been previously used for shuttering, deshuttering, or for plotting motives on a horizontal surface that would then be used as guides to place shutter profiles [27], [28].

2) *Instrumented segmental tunnels*

While the use of robotics for civil asset inspection is becoming increasingly common [29]-[35], the application of robotics to deploy fixed sensors on concrete structures is not as prevalent [36]. The deployment of sensors in tunnel segments, as seen in [12], [37]-[40], is achieved manually.

Sensors based on fibre-optic and, most commonly, vibrating wire physical principles have been widely used to measure various parameters, including structural deformations, cracking, and, most commonly, strains. The assessment of instrumented segments involves comparing strain or displacement generated from a compression or a three-point-bending test with analytical or numerical models to validate design assumptions or better understand specific cases.

3) *Vibrating wire strain gauge (VWSG)*

VWSGs are commonly used sensors in civil infrastructures, especially for embedding into concrete. The operation principle of a VWSG, shown in Fig. 1, is based on the principle of a vibrating wire whose resonating frequency, obtained through electromagnetic pulses sent by a coil attached to the sensor, can be correlated to the strain as show in Equation (1), where ε is the strain, K the strain factor, and f the resonant frequency.

$$\varepsilon = K.f^2 \tag{1}$$

VWSGs are widely available and present excellent features, such as durability and high accuracy, making them attractive strain sensors for concrete applications.

II. METHODOLOGY

A. Sensor node components and packaging design

For this work, we have developed an embeddable VWSG sensing node. The design is compatible with a fully wireless system; however, in this work we used a wired system for interrogation.

The VWSGs used (Geokon 4202) are usually recommended for lab-based applications on micro concrete (aggregate size less than 10 mm) and mortar. The sensors provide strain measurements and are equipped with a thermistor that collects temperature data for temperature compensation.

As shown in Fig. 2, our sensing node consisted of the VWSG, an addressable board for processing, an Arduino Nano microcontroller for signal interpretation via Modbus, communication, and storage. Power and communications were delivered via a wired connection between the microcontroller and a laptop in this work, but the system is also compatible with a battery-operated setup.

This sensing node needed to be embedded within robust, waterproof packaging and be compatible with the robotic pick-and-place (PnP) process. For this we designed the 3D-printed sensor enclosure shown in Fig. 3. Production need not necessarily rely on 3D printing, but it is a suitable choice for lab-based work during the design stage. The interrogating electronics sat within the box, at its base, with the VWSG fitted across two protrusions. The base of the box was equipped with neodymium magnets, allowing the sensor node to be fixed securely to the steel formwork and remain in place during concrete vibration.

B. Robotic deployment of wireless node

To our knowledge, accepted methodologies for evaluating the precision and accuracy of robotic PnP operations in a construction context do not yet exist. Benchmarking frameworks exist in other sectors however, notably in the food industry [41]-[42]. The cited frameworks introduce four pertinent evaluation metrics for PnP:

- The success rate, calculated as the ratio of successful PnP instances to the total attempts made.
- The mean picks per hour.
- The successful task executions over total attempts, serving as an approximation of the probability of achieving successful task execution in a single attempt.

This article has been accepted for publication in IEEE Sensors Journal. This is the author's version which has not been fully edited and content may change prior to final publication. Citation information: DOI 10.1109/JSEN.2025.3559405

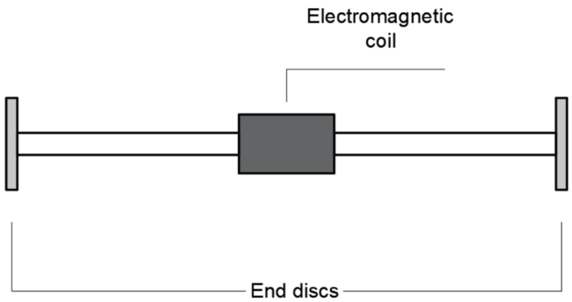

Fig. 1. Schematic representation a vibrating wire strain gauge.

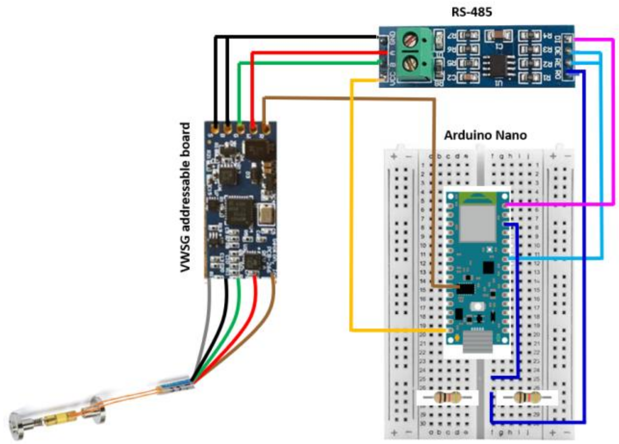

Fig. 2. Pinout of vibrating wire strain gauge (VWSG) interrogation system

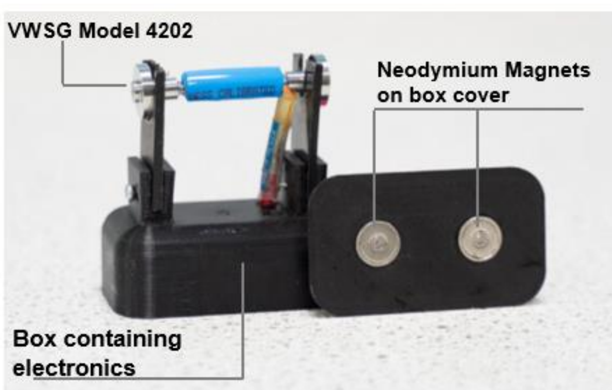

Fig. 3. VWSG box

- The average duration and standard deviation of duration for successful PnP cycles.

While these metrics are apt for comprehensively assessing PnP systems in scenarios such as accurate fruit placement within bins, they are population statistics that are not exhaustive when it comes to assessing the placement precision of each item individually. As such, we extended this framework in this work.

1) *Geometric error evaluation*

Our objective was to achieve precise, accurate sensor node deployment while minimizing geometric deviations. To assess deployment accuracy, sensor nodes were robotically placed onto the steel segment formwork. A camera setup recorded the final position of the sensor enclosure showing its relative location in position ΔX, ΔY, and angle ΔΘ compared to an ideal target location. This was repeated over 100 iterations, allowing us to statistically evaluate the translation and rotational errors.

Fig. 4 presents the experimental layout of the robotic deployment of the sensors. On one side, the robotic arm (equipped with an adapted gripper) picked up the wireless node from a designated point and placed it on the other side on a steel plate with a clearly distinguishable printed target (identically shaped to the box). This process was repeated 100 times for the following scenarios to provide comparison:

- Robotic PnP with magnet (RWM)
- Robotic PnP without magnet (RWOM)
- Manual PnP with magnet (MWM)
- Manual PnP without magnet (MWOM)

The robotic PnP process took 585 seconds to complete at a maximum speed of 1 m/s of the UR for each scenario while the manual process took 610 seconds.

At the end of each process of individual PnP, a high-resolution picture of the box was taken showing its position relative to the printed target. The picture was stored for further analysis. A series of image processing techniques were then applied to automatically calculate the spatial deviation of the box from its desired location:

i. Firstly, the captured images were converted to greyscale with pixel intensities ranging from 0 (black) to 255 (white).
ii. The Otsu thresholding method, an image processing algorithm, was then applied to produce a binary image, segmenting the box from the background.
iii. A bounding box was then mapped to the extremities of the contours of the segmented box. The centre of both boxes was taken as the intersection of the horizontal and vertical axis.
iv. The coordinates of this centre point were then subtracted from the coordinates of the centre of the target, resulting in ΔX and ΔY. The angle of rotation was calculated using simple trigonometry.

While our final application involves curved elements (precast tunnel segment formwork), for simplicity, a flat metallic surface was used to perform the assessment of repeatability in this work. Results obtained in this manner can be transposed to curved surfaces, given the large size (and hence low curvature) of real segment moulds.

2) *Geometrical error impact on strain error*

There is an intrinsic relationship between geometrical and strain errors. Translational errors' impacts on expected strain will depend on the segment's geometry and its final loading, but these will be, relative to the segment's size, very small, and so of secondary importance to errors in placement angle. For a unitary strain, the change in the angular deviation (ΔΘ) leads to a change in the value of strain as expressed in Equation (2). The strain relative change expressed in percentage is shown in Equation (3).

$$\varepsilon' = \frac{\varepsilon}{2}(1 + \cos 2\Delta\theta) \tag{2}$$

$$\frac{\Delta\varepsilon}{\varepsilon}(\%) = \frac{\varepsilon' - \varepsilon}{\varepsilon}.100 \qquad (3)$$

C. Smart segment

1) Smart segment

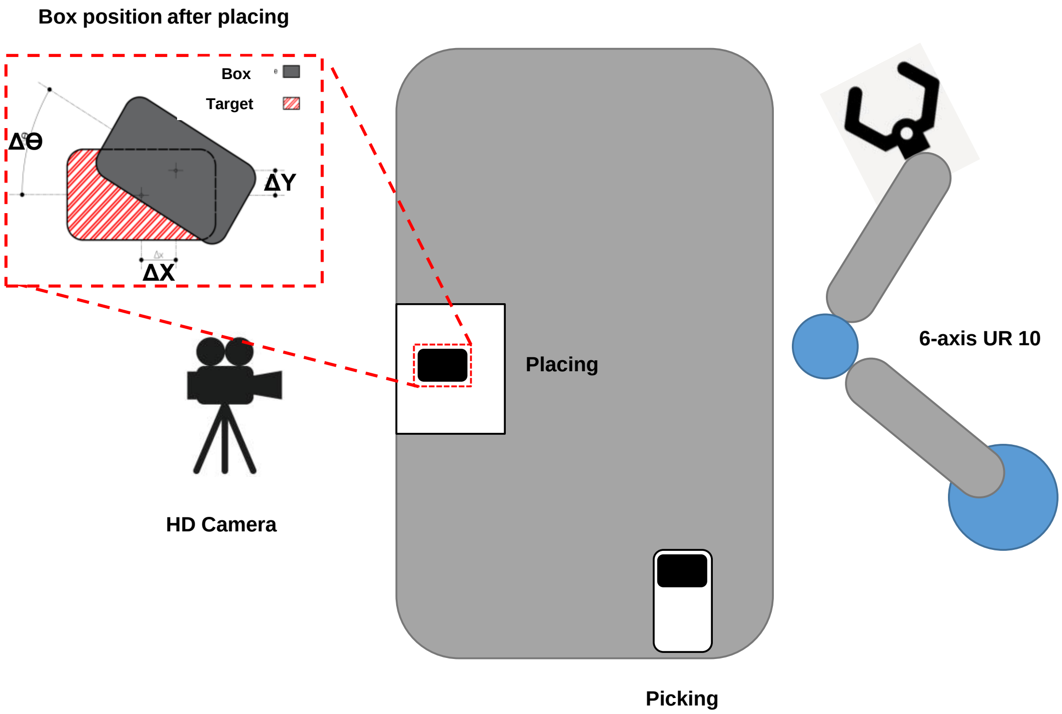

Fig. 4. Schematic layout of the PnP of the box. On the top left is the photo captured after robotically placing the box. The rest of the figure shows the 6-axis universal robot with a 10 kg payload (UR-10), the table on which the robotic PnP is performed, and the position of the box before picking.

In this work, we used the early design geometry of the Lower Thames Crossing (LTC) project [43] to inform the design of our lab-scale segment geometries and concrete mixes. The full-scale segment was downsized by a factor of five (applied to both the segment thickness and length), taking into account factors such as: (i) the loads imposed during casting, transport, and testing stages; (ii) the actual aggregate size; and (iii) the dimensions of the sensors to be embedded [44].

To mimic the LTC project's mix design, the lab-scale segment was made from steel fibre reinforced concrete (SFRC), the composition of which is presented in TABLE I. The average SFRC compression obtained by testing 28 days cured 100 mm cubes [45] was 40.3 MPa. The average maximum flexural strength obtained testing 500 mm x 100 mm x 100 mm beams [46] was 4.39 MPa.

Sensor nodes were embedded ~~placed~~ in segments using robotic PnP to deploy them on the empty formwork (see Fig. 5) before concrete was poured and cured for 28 days. Each segment mould measured 1080 x 245 x 110 mm and included an instrumented and a non-instrumented segment.

2) Preliminary tests on straight beam

Before characterising the smart segment, we performed a preliminary evaluation on 100 x 100 x 500 mm beams made from the same type of concrete as the smart segment, as it is an easier system to analyse.

The experimental layout included the following components:

- The instrumented beam, featuring two vibrating wire strain gauges. One VWSG was embedded within the beam, while the second was surface-mounted at the bottom.
- An ad hoc data acquisition system, as previously presented in Fig. 2 was utilized to interrogate the sensors during the bending test and transmit data to an independent computer.
- A universal test machine was employed to execute a customized flexural test. Additionally, two linear variable differential transformers (LVDTs) were positioned at the midspan to measure the average displacement.

The test procedure involved the application of a gradual concentrated load at the midspan, ranging from 0.5–2.5kN initially, followed by 0.5–3.5kN. This sequence was repeated ten times. The objective was to analyse the preliminary results obtained from the simplified model and gain insight into the expected outcomes for lab-scale tunnel segments. Furthermore, the surface mounted VWSG and the LVDT measurements at midspan serve as reference values to validate the performance of other sensors within smart segments.

3) Smart segment characterisation

The characterisation consisted of evaluating the repeatability of strain measurement across ten smart segments. This was done through statistical evaluation of the strain transfer: this is defined as the percentage of strain transferred from the material (concrete) to the sensors.

The process starts with the casting of two segments, with one incorporating VWSGs through robotic deployment, while the other remains uninstrumented. The accurate placement of sensor boxes is ensured by marking specific locations on the formwork to maintain consistency across the smart segments.

Smart segments consisted of a curved beam with a 900 mm span equipped with embedded and surface-mounted instrumentation. As with the straight beam, the test was a load-

Fig. 5. Sensor node being placed in the formwork with a universal robot UR10

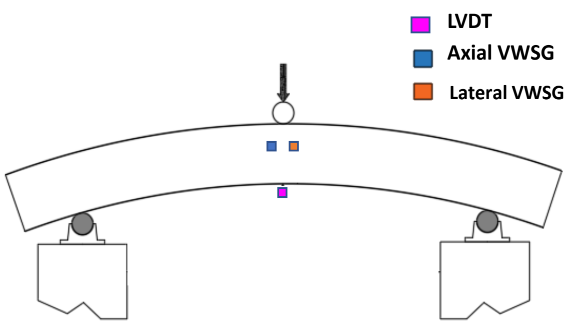

Fig. 6. Smart segment three-point bending test layout.

controlled three-point bending with its setup illustrated in Fig. 6.

After both segments reach maturity (28 days of curing), a 3-point bending failure test is conducted on the plain segment, and the resulting value is recorded. A cyclical three-point bending test was later performed on the instrumented segment, with loading capped at 50% of the average failure loads from the plain segment test. Throughout this phase, loads, displacements at midspan, and strain values were recorded.

The experimental layout included the following components:

- The instrumented beam, featuring two embedded VWSGs, located slightly above the centre of gravity.
- An ad hoc data acquisition system, as described earlier, to interrogate the sensors.

TABLE I
STEEL FIBRE REINFORCED CONCRETE MIX COMPOSITION PER CUBIC METRE OF CONCRETE

Components	Quantity	Unit
Cement (CEM II 32.5R)	350	[kg]
Water	158	[l]
Coarse aggregate (10 mm)	1200	[l]
Sand	600	[kg]
Fibres	40	[kg]
Superplasticiser	1.4	[l]

- A universal test machine was employed to execute a customized flexural test.

Additionally, two LVDTs were positioned at the midspan to measure the average displacement.

The test procedure involved the application of a gradual and sequential concentrated load at the midspan, ranging from 0.5–5.5 kN. Similar to the straight beam, the load was sequentially increased and decreased in a cyclical manner, obtaining a total of 10 cycles per beam tested.

In parallel to the fabrication and testing of the lab-scale segments, and in order to later determine strain transfers, the development of a numerical model was conducted to mimic the loading conditions on the instrumented segment. In this study the use of a finite element model (FEM) was preferred to an analytical model obtained by approximating the curved beam with an equivalent straight beam. The later approach does not fully capture the structural behaviour due to the curvature.

Finally, the repeatability of the smart segment with robotically deployed sensors was assessed in two steps:

1. Plot scatterplot of peak values of measured strains versus calculated strains using the FEM. The strain transfer which is the ratio between the latter and the former is determined for each instrumented segment.
2. The repeatability of strain transfers across the 10 segments is evaluated using statistical metrics, including the coefficient of variation and the Intraclass Correlation Coefficient (ICC) of the strain transfer for robotically deployed VWSGs. The ICC, commonly utilized in reliability studies, serves as a robust means to gauge the consistency and agreement among repeated measurements, offering an objective indicator of the repeatability of strain measurements.

This article has been accepted for publication in IEEE Sensors Journal. This is the author's version which has not been fully edited and content may change prior to final publication. Citation information: DOI 10.1109/JSEN.2025.3559405

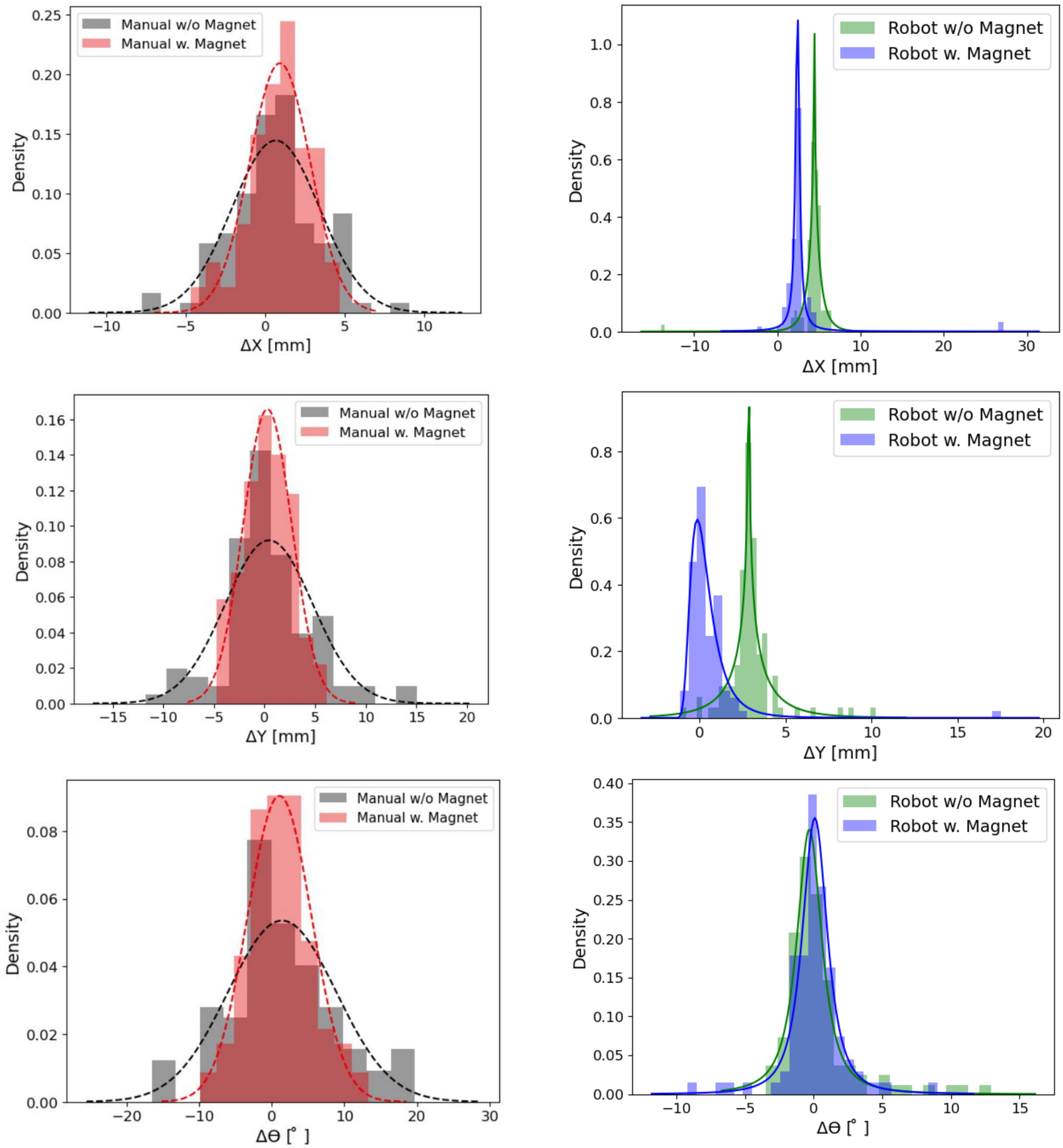

Fig. 7. Statistical distributions of geometric errors ΔX, ΔY, and ΔΘ for the manual and robotic scenarios. The density is expressed as the relative frequency of observations (ΔX, ΔX, and ΔΘ) adjusted so that the total area under the histogram sums to 1.

III. RESULTS

A. Robotic PnP evaluation

1) *Geometric errors*

TABLE II presents the results of the geometric and strain errors of robotic and manual PnP. Similarly, Fig. 7 shows the distributions of geometric errors across manually and robotically deployed sensor nodes, with and without the use of magnetic attachment. The graphs display a consistent trend across the three geometric parameters: the deployment of sensors via robotics significantly reduced dispersion when compared to manual deployment. Additionally, the introduction of magnets enhanced precision, yielding a more tightly clustered distribution in both manual and robotic contexts. Both the linear (ΔX ,ΔY) and angular deviations ($\Delta\theta$) follow Normal distributions in all scenarios, except for ΔY in RWM (Robot With Magnet), which follows a Gamma distribution. This right-skewed behaviour suggests a systematic effect of the magnet on robotic motion, warranting further investigation.

This article has been accepted for publication in IEEE Sensors Journal. This is the author's version which has not been fully edited and content may change prior to final publication. Citation information: DOI 10.1109/JSEN.2025.3559405

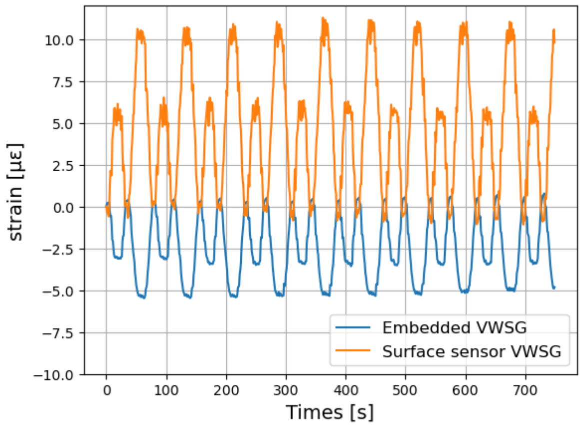

Fig. 8. Drift corrected strains timeseries from 3-point bending test on prismatic straight beam

While the impact of the magnetic box sensor enclosure is less debatable, we should be aware of the limitations of this study when it comes to comparing manual to robotic deployment. The manual placement was done by the authors, who are subject to bias in favour of showing that the robotic placement process is superior. The distributions for manual placements do at least fit to Gaussian probability density functions, which can give us some indication that they are not subject to significant bias; nevertheless, future work should aim to repeat the manual placement method, ideally using a broader population of more independent subjects (e.g., precast factory employees).

The examination of theoretical strain losses across the four scenarios reveals a consistent trend: robotic magnetic deployment has the potential to reduce errors and the variability in those errors when compared to manual and non-magnetic placement. These results collectively emphasize the potential of robotics to add robustness and consistency to sensor deployment in a precast manufacturing context.

B. Smart segment

1) *Prismatic smart beam*

The VWSG strains presented a noticeable drift over time, a consequence of machine drift that was corrected for. Fig. 8. shows the strain time series on a typical smart segment where the repetitive pattern during the load controlled three-point bending tests is reflected in the measurement.

The simple prismatic beam finite element (FE) model of the beam was loaded with identical loads as the one during the test. Once built, the model was iteratively calibrated (changing values of E the Young's modulus and ν Poisson's ratio) until the calculated displacements were close to the measured ones. After this exercise, the respective values of E and ν were estimated to be 30 GPa and 0.2, sensible values that agree with the low-load linear portion of concrete's mechanical response.

A comparison between strain values measured during the test and the ones obtained with the FE model can shed more preliminary insights. Such comparison can be done by evaluating the strain transfer, the relation between the actual strain in the concrete and the strain measured by the sensor. Based on the FE model and the strain results, we can estimate the strain transfer coefficient for the sensors in the straight beam. The strain transfer— the ratio of theoretical strain to the measured strain at the measurement position—for the embedded and surface mounted VWSG sensors was 0.53 and 0.71, respectively.

TABLE II
GEOMETRIC AND STRAIN ERRORS OF ROBOTIC PNP VS MANUAL PNP

Scenario	(ΔX) [mm]	(ΔY) [mm]	ΔΘ [deg]	Strain error [%]
MWOM	0.68 ± 2.76	0.44 ± 4.34	1.44 ± 7.45	1.72± 2.53
MWM	0.94 ± 1.91	0.29 ± 2.41	1.08 ± 4.41	0.62± 0.99
RWOM	4.50 ± 0.44	2.86 ± 0.86	-0.30 ± 1.01	0.23± 0.70
RWM	2.39 ± 2.89	-0.027 ± 0.63	0.098 ± 0.99	0.14± 0.41

2) *Smart tunnel segment (curved beam)*

This part of the study aimed to analyse the repeatability of strain measurements in smart segments under varying loading conditions. This investigation is crucial for assessing the reliability of strain measurement techniques in tunnel smart segments.

Data was collected from ten different smart segments, each subjected to the same loading scenarios. Drift-corrected strain measurements (Fig. 9) were recorded for the two different strain gauges, and calculated strains were derived from load measurements. The calculated strains were obtained using an FE model of the three point-bending test that mimicked the actual test, the FE model is shown in Fig. 10.

Fig. 11 presents a scatterplot illustrating the strain measurements against the corresponding strain calculations obtained through numerical modelling. The gradient of the regression line, which intersects the origin, is the strain transfer coefficient. A value of 1.0 would indicate an exact match between measured and predicted strains; therefore, the closer this value is to 1, the better. Notably, the average strain transfer coefficients for the longitudinal and transversal VWSGs across all 10 experiments stand at 0.93 ± 0.012 and 0.567 ± 0.011 respectively, with errors quoted as the standard deviation across the sample. The value 0.93 is relatively close with the difference explained by differences in real behaviour of the concrete versus idealised behaviour in the model. Assessing the repeatability of this measurement across all ten smart segments, the coefficient of variation unveils consistently stable strain measurements, with values of 1% for the longitudinal VWSG and 1.9% for the transverse VWSG.

The observed strain transfer values slope in both VWSGs indicate a consistent and reliable relationship between calculated and measured strains. This suggests that the calculated strains based on load measurements provide an accurate estimate of the actual strains experienced by the smart segments. We posit that the variability in the values of the strain transfer in both VWSGs can be attributed to the position variations in the casting of the segments in the lab, rather than translational or geometrical errors in the sensor placement (as our results in TABLE II show that the strain errors resulting from robotic placement are likely 1%). Future work should therefore seek to re-assess strain transfer for real smart segments cast in a factory, as these will undoubtedly be more repeatable than those cast manually in a lab. It is however, also possible that the sensors or actual position of the transversal sensors (VWSG2) has shifted during vibration of the concrete in the segment. Future work could therefore look to assess the final location of sensors after casting, through x-ray imaging or destructive testing.

The Intraclass Correlation Coefficient (ICC) was also

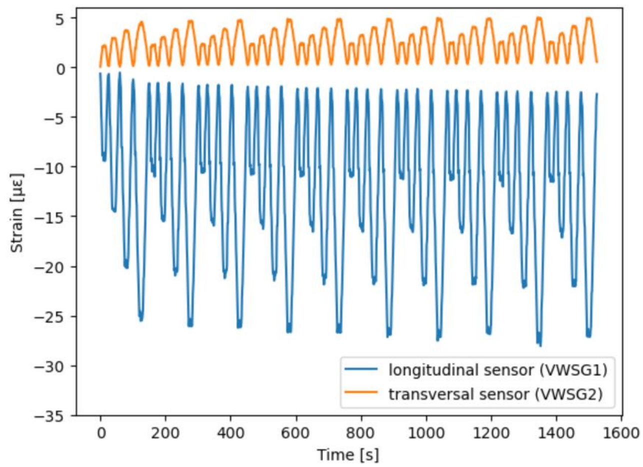

Fig. 9. Strains time series captured from longitudinal and transversal VWSG.

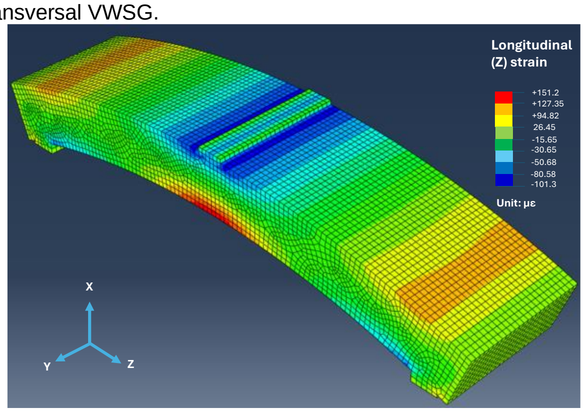

Fig. 10. FE model of a Curved beam showing the longitudinal strains generated with Abaqus.

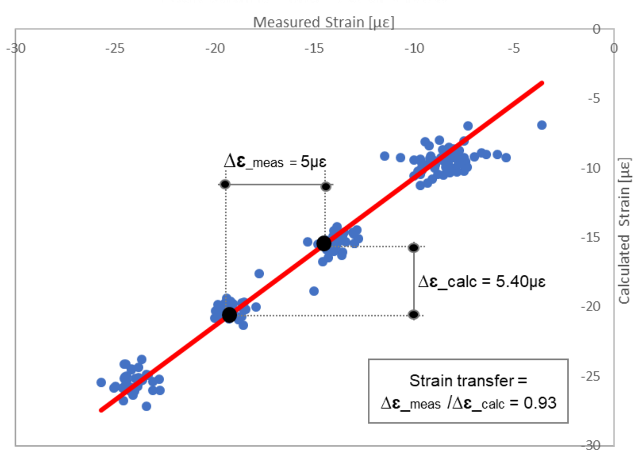

Fig. 11. Strain transfer determination.

utilized to assess the agreement between measurements of peak strains (VWSGs 1 and 2). The ICC a statistical metric used to assess the proportion of total variance in a dataset that is attributed to the variability between different groups or categories, indicating the degree of agreement or consistency among these groups. The average ICC values across the 10 smart segments is 0.795 for VWSG 1 and 0.396 for VWSG 2. This confirms the previous observation found using the coefficient of variation as a repeatability metric.

The significantly lower strain-transfer coefficient for the lateral VWSG (when compared to the longitudinal) is most likely due to the sensor's final position shifting after concrete casting and vibration. Unlike the longitudinal sensor, which was directly on top of the electronic box (proving more stability), the lateral sensor was positioned at the end of a cantilever, making it more prone to movement, despite precautions taken, during casting. Additionally, because we had curved beam, the transversal strain is affected by second order factors not entirely taken into account in the theoretical model. While these two observations guarantee further investigation, the value (superior to 0.50) remains adequate and the dispersion across the tested segments shows a consistent pattern of lower errors.

IV. CONCLUSION

This paper demonstrates an automated sensor deployment process for lab-scale precast tunnel segments, specifically employing a collaborative robotic arm for VWSG sensor deployment. Robotic sensor deployment exhibited significantly improved accuracy and consistency compared to manual methods. Strain errors originating from angular geometric variations were minimized to less than 1% through robotic deployment, further bolstered by the inclusion of magnets in sensor packaging, which notably enhanced precision.

Our study also unveiled consistent strain transfer coefficients for embedded sensors in smart segments, with average values of 0.93 for longitudinal strain and 0.567 for transversal strain. Moreover, we confirmed the repeatability of strain measurements within these segments, demonstrating coefficient of variation values of 1% for longitudinal sensors and 1.9% for transversal sensors. High interclass correlation coefficients of 0.795 for longitudinal sensors and 0.396 for transversal sensors further affirmed the reliability of the robotic technology employed.

These findings, derived from a controlled lab-scale environment, highlighted the effectiveness of using robotic technology for sensor deployment. This approach not only demonstrated potential in the improvement of productivity but also showed enhanced reliability of manufacturing smart tunnel segments. Additionally, the research made a strong case for the early adoption the SHM in precast elements, as it enabled the monitoring of pre-construction structural behaviour, crucial in the design SFRC tunnel segments increasingly used in new tunnel projects. Future works involve implementing a study on a full-scale smart segment to assess the repeatability of the robotic process in strain transfers across a larger sample of segments, thereby further advancing understanding in this area.

V. ACKNOWLEDGEMENTS

This work was supported by COWI Ltd UK, National Highways, and the Scottish Research Partnership for Engineering.

VI. REFERENCES

[1] The British Tunnelling Society and The Institution of Civil Engineers, '2 Project definition', in *Tunnel lining design guide*, Thomas Telford Publishing, 2004, pp. 8–19. doi: 10.1680/TLDG.29866.0002.

[2] The British Tunnelling Society and The Institution of Civil Engineers, '4 Design life and durability', in *Tunnel lining design guide*, Thomas Telford Publishing, 2004, pp. 40–58. doi: 10.1680/TLDG.29866.0004.

[3] Geokon Inc., 'Model 4200 Series Vibrating Wire Strain Gages Instruction Manual', 2018, [Online]. Available: https://www.geokon.com/content/manuals/4200-4202-4204-4210_Strain_Gages.pdf

[4] M. Alhaddad, M. J. Wilcock, C. Y. Gue, K. Soga, M. Devriendt, and M. Dewhirst, 'Cast-iron tunnels' tolerance to imposed longitudinal settlement curvature', *Geotechnique*, vol. 71, no. 11, pp. 1044–1055, Nov. 2021, doi: 10.1680/JGEOT.18.P.182/ASSET/IMAGES/SMALL/JGEOT.18.P.182-F12.GIF.

[5] M. Alhaddad, M. D. Meng, K. Soga, and M. Devriendt, 'A new photogrammetric system for high-precision monitoring of tunnel deformations', 2019, doi: 10.1680/jtran.18.00001.

[6] N. De Battista *et al.*, 'Strain monitoring using embedded distributed fibre optic sensors in a sprayed concrete tunnel lining during the excavation of cross-passages Smart Infrastructure View project ITN-FINESSE Innovative Training Network on optical fiber sensors View project St', 2015. Accessed: May 20, 2021. [Online]. Available: https://www.researchgate.net/publication/303386310

[7] D. Rodenas Herráiz, K. Soga, P. R. A. Fidler, and N. de Battista, 'London Underground tunnel lining replacement monitoring (UK)', *Wireless Sensor Networks for Civil Infrastructure Monitoring*, pp. 1–6, 2016, doi: 10.1680/WSNCIM.61514.173.

[8] H. Mohamad *et al.*, 'Monitoring Twin Tunnel Interaction Using Distributed Optical Fiber Strain Measurements', 2012, doi: 10.1061/(ASCE)GT.1943-5606.0000656.

[9] H. Mohamad, P. J. Bennett, K. Soga, R. J. Mair, and K. Bowers, 'Behaviour of an old masonry tunnel due to tunnelling-induced ground settlement', *Geotechnique*, vol. 60, no. 12, pp. 927–938, Dec. 2010, doi: 10.1680/geot.8.P.074.

[10] B. Moritz, R. Heissenberger, T. Schachinger, and W. Lienhart, 'Long-term monitoring of railway tunnels', *Geomechanik und Tunnelbau*, vol. 14, no. 1, pp. 35–46, Feb. 2021, doi: 10.1002/geot.202000049.

[11] C. M. Monsberger and W. Lienhart, 'Distributed fiber optic shape sensing along shotcrete tunnel linings: Methodology, field applications, and monitoring results', *J Civ Struct Health Monit*, vol. 11, no. 2, pp. 337–350, Apr. 2021, doi: 10.1007/s13349-020-00455-8.

[12] P. Gehwolf *et al.*, 'Deformation measurements of tunnel segments at a newly developed test rig / Deformationsmessungen an Tübbingen mit einem neu entwickelten Prüfstand', *Geomechanik und Tunnelbau*, vol. 9, no. 3, pp. 180–187, Jun. 2016, doi: 10.1002/geot.201600012.

[13] C. M. Monsberger, W. Lienhart, and B. Moritz, 'In-situ assessment of strain behaviour inside tunnel linings using distributed fibre optic sensors: Beurteilung des In-situ-Dehnungsverhaltens der Tunnelschale mittels verteilter faseroptischer Messsysteme', *Geomechanik und Tunnelbau*, vol. 11, no. 6, pp. 701–709, Dec. 2018, doi: 10.1002/geot.201800050.

[14] L. Wagner *et al.*, 'Direct and Distributed Strain Measurements Inside a Shotcrete Lining: Concept and Realisation', *Rock Mech Rock Eng*, vol. 53, no. 2, pp. 641–652, Feb. 2020, doi: 10.1007/s00603-019-01923-4.

[15] F. Michelin, A. Nahli, V. Lamour, and T. D. Le, 'Holistic approach for the construction monitoring of the Grand Paris Express metro network', *Lecture Notes in Civil Engineering*, vol. 62, pp. 265–272, 2020, doi: 10.1007/978-981-15-2184-3_33.

[16] J. Gómez, J. R. Casas, and S. Villalba, 'Structural Health Monitoring with Distributed Optical Fiber Sensors of tunnel lining affected by nearby construction activity', *Autom Constr*, vol. 117, p. 103261, Sep. 2020, doi: 10.1016/j.autcon.2020.103261.

[17] A. Barrias, G. Rodriguez, J. R. Casas, and S. Villalba, 'Application of distributed optical fiber sensors for the health monitoring of two real structures in Barcelona', *https://doi.org/10.1080/15732479.2018.1438479*, vol. 14, no. 7, pp. 967–985, Jul. 2018, doi: 10.1080/15732479.2018.1438479.

[18] X. Wang *et al.*, 'Structural deformation monitoring during tunnel construction: a review', *J Civ Struct Health Monit*, vol. 14, no. 3, pp. 591–613, Mar. 2024, doi: 10.1007/S13349-023-00741-1/METRICS.

[19] J. Gómez, J. R. Casas, and S. Villalba, 'Structural Health Monitoring with Distributed Optical Fiber Sensors of tunnel lining affected by nearby construction activity', *Autom Constr*, vol. 117, p. 103261, Sep. 2020, doi: 10.1016/J.AUTCON.2020.103261.

[20] B. Glišić and Daniele. Inaudi, *Fibre optic methods for structural health monitoring*. John Wiley & Sons, 2007.

[21] M. Gharbia, A. Y. Chang-Richards, and R. Y. Zhong, 'Robotic technologies in concrete building construction: A systematic review', in *Proceedings of the 36th International Symposium on Automation and Robotics in Construction, ISARC 2019*, International Association for Automation and Robotics in Construction I.A.A.R.C), 2019, pp. 10–19. doi: 10.22260/isarc2019/0002.

[22] B. Nematollahi, M. Xia, and J. Sanjayan, 'Current progress of 3D concrete printing technologies', in *ISARC 2017 - Proceedings of the 34th International Symposium on Automation and Robotics in Construction*, International Association for Automation and Robotics in Construction I.A.A.R.C), 2017, pp. 260–267. doi: 10.22260/isarc2017/0035.

[23] T. Bock and T. Linner, *Robot-Oriented Design*. New York: Cambridge University Press, 2015. doi: 10.1017/CBO9781139924146.

[24] T. Bock and T. Linner, *Robotic industrialization : automation and robotic technologies for customized component, module, and building prefabrication*. Cambridge: Cambridge University Press, 2015.

[25] T. Bock and T. Linner, *Robot-oriented design : design and management tools for the deployment of automation and robotics in construction*.

[26] T. Bock, 'Construction Automation and Robotics', 2008. doi: 10.5772/5861.

[27] Weckenmann, 'All products'. Accessed: Feb. 06, 2020. [Online]. Available: https://weckenmann.com/en/products/all-products

[28] H. Formwork, 'Automated Segment Production'.

[29] T. McDonald, M. Robinson, and G. Y. Tian, 'Developments in 3D Visualisation of the Rail Tunnel Subsurface for Inspection and Monitoring', Nov. 01, 2022, *MDPI*. doi: 10.3390/app122211310.

[30] S. Halder and K. Afsari, 'Robots in Inspection and Monitoring of Buildings and Infrastructure: A Systematic Review', Feb. 01, 2023, *MDPI*. doi: 10.3390/app13042304.

[31] H. Ahmed, H. M. La, and N. Gucunski, 'Review of non-destructive civil infrastructure evaluation for bridges: State-of-the-art robotic platforms, sensors and algorithms', Jul. 02, 2020, *MDPI AG*. doi: 10.3390/s20143954.

[32] I. Katsamenis *et al.*, 'Robotic Maintenance of Road Infrastructures: The HERON Project', in *ACM International Conference Proceeding Series*, Association for Computing Machinery, Jun. 2022, pp. 628–635. doi: 10.1145/3529190.3534746.

[33] B. Bendris and J. C. Becerra, 'Design and Experimental Evaluation of an Aerial Solution for Visual Inspection of Tunnel-like Infrastructures', *Remote Sensing 2022, Vol. 14, Page 195*, vol. 14, no. 1, p. 195, Jan. 2022, doi: 10.3390/RS14010195.

[34] F. Ahmed, J. C. Mohanta, A. Keshari, and P. S. Yadav, 'Recent Advances in Unmanned Aerial Vehicles: A Review', *Arab J Sci Eng*, vol. 47, no. 7, pp. 7963–7984, Jul. 2022, doi: 10.1007/s13369-022-06738-0.

[35] M. R. Khosravani and A. Haghighi, 'Large-Scale Automated Additive Construction: Overview, Robotic Solutions, Sustainability, and Future Prospect', *Sustainability (Switzerland)*, vol. 14, no. 15, Aug. 2022, doi: 10.3390/su14159782.

[36] J. McAlorum, M. Perry, C. Vlachakis, L. Biondi, and B. Lavoie, 'Robotic spray coating of self-sensing metakaolin geopolymer for concrete monitoring', *Autom Constr*, vol. 121, p. 103415, Jan. 2021, doi: 10.1016/j.autcon.2020.103415.

[37] N. Radončić, M. Kern, M. Weissnar, and B. Moritz, 'Dehnmessgeber in Tübbingsegmenten - Funktionsweise, Auswertung und Interpretation', *Geomechanik und Tunnelbau*, vol. 8, no. 3, pp. 265–272, Jun. 2015, doi: 10.1002/geot.201500004.

[38] T. Qi, X. Liang, Z. Jin, and W. Qian, 'An experimental approach to evaluating the long-term performance of segmental linings', *International Journal of Physical Modelling in Geotechnics*, vol. 21, no. 3, pp. 150–167, May 2021, doi: 10.1680/JPHMG.19.00038.

[39] K. Kesavan, K. Ravisankar, S. Parivallal, P. Sreeshylam, and S. Sridhar, 'Experimental studies on fiber optic sensors embedded in concrete', *Measurement (Lond)*, vol. 43, no. 2, pp. 157–163, Feb. 2010, doi: 10.1016/j.measurement.2009.08.010.

[40] W.-C. Cheng, J. C. Ni, and S.-L. Shen, 'Experimental and Analytical Modeling of Shield Segment under Cyclic Loading', *International Journal of Geomechanics*, vol. 17, no. 6, p. 04016146, Jun. 2017, doi: 10.1061/(ASCE)GM.1943-5622.0000810.

[41] P. Triantafyllou, H. Mnyusiwalla, P. Sotiropoulos, M. A. Roa, D. Russell, and G. Deacon, 'A benchmarking framework for systematic evaluation of robotic pick-and-place systems in an industrial grocery setting', *Proc IEEE Int Conf Robot Autom*, vol. 2019-May, pp. 6692–6698, May 2019, doi: 10.1109/ICRA.2019.8793993.

[42] H. Mnyusiwalla *et al.*, 'A Bin-Picking Benchmark for Systematic Evaluation of Robotic Pick-and-Place Systems', *IEEE Robot Autom Lett*, vol. 5, no. 2, pp. 1389–1396, Apr. 2020, doi: 10.1109/LRA.2020.2965076.

[43] N. Highways, 'What is the Lower Thames Crossing? - National Highways', Jun. 2022, Accessed: Feb. 14, 2023. [Online]. Available: /our-roads/lower-thames-crossing/what-is-the-lower-thames-crossing/

[44] J. Tuset, J. Pera, and J.-C. Cubaud, 'Etude de modèles réduits de structures en micro-béton armé', *Bulletin technique de la Suisse romande*, 1973.

[45] British Standards, 'BS EN 12390-3:2019: Testing hardened concrete: Compressive strength of test specimens', 2019, *British Standards Institute*.

[46] British Standards, 'BS EN 14651:2005 +A1:200: Test method for metallic fibre concrete — Measuring the flexural tensile strength (limit of proportionality (LOP), residual)', vol. 3, pp. 1–17, 2007.

Tresor Tshimbombo is a Ph.D. researcher in the Department of Civil and Environmental Engineering at the University of Strathclyde. His research focuses on developing robotic solutions for deploying sensors into concrete elements. Tresor earned his B.Sc. in Civil Engineering from the University of Kinshasa and has since been actively involved in academia, teaching courses at both the University of Kinshasa and the University of Strathclyde. His expertise extends to areas such as concrete mix design, reinforced concrete design, structural analysis, and soil mechanics. In addition to his academic pursuits, he brings valuable industry experience to his research. He worked as a project manager in the construction industry for five years.

This article has been accepted for publication in IEEE Sensors Journal. This is the author's version which has not been fully edited and content may change prior to final publication. Citation information: DOI 10.1109/JSEN.2025.3559405

Dr Marcus Perry is a Senior Lecturer in the department of Civil and Environmental Engineering, University of Strathclyde. He has around 10 years of combined academic and industry experience developing fibre-optic, wireless, and self-sensing material sensor networks and imaging inspection methods for civil infrastructure. His industry collaborators span transport, nuclear and renewables sectors.

Hamish Dow is a Ph.D. student in the Department of Civil and Environmental Engineering at the university of Strathclyde, focusing on the use of robotic and aerial drones' solutions for detailed inspections of concrete and steel structures. His research is a blend of civil engineering, computer science, electrical engineering, photography, and 3D printing.

Dr Jack McAlorum currently worked for 5 years at the Department of Civil and Environmental Engineering (CEE), University of Strathclyde as a Postdoc specialising on sensor development for structural health monitoring, automated inspections, including the development of a bespoke illumination platform and implementation of white-box and black-box algorithms for crack detection.

Dr Chris Hoy, in his role as the Director responsible for the structures team, plays a pivotal role in major projects worldwide, including the Thames Tideway, Lower Thames Crossing, High Speed 2 in the UK, and the Deep Tunnel Sewerage System Phase 2 (DTSS2) in Singapore. With over two decades of experience, Chris specializes in delivering economically viable and safely buildable detailed designs for diverse engineering projects. His expertise spans tunnels, wind turbine foundations, railway structures, minor highway bridges, water retaining structures, and buildings. Chris's focus includes collaboration with contractors, clients, and designers, ensuring adherence to design standards within COWI UK Tunnels division. As a Chartered Civil Engineer and Structural Engineer, he brings a wealth of knowledge in specialist concrete structures, soil-structure interaction, non-linear material behaviour, and cyclic loading, showcasing his dedication to advancing engineering solutions.

Dr Chrysoula Litina serves as the Principal Research Engineer at National Highways (UK), where she channels her passion for research innovation in construction materials and the integration of new technologies in infrastructure. A staunch STEM advocate, Chrysoula is committed to advancing the field through her expertise and advocacy efforts. With a Doctor of Philosophy (Ph.D.) in Civil Engineering from the University of Cambridge (UK), Chrysoula possesses a solid academic foundation. Her journey includes an MSc in Hydraulic and Environmental Engineering, as well as BEng and MEng degrees from Democritus University of Thrace (Greece).